Available online at www.sciencedirect.com
ScienceDirect
Talanta 74 (2008) 1659–1669
Talanta
www.elsevier.com/locate/talanta

Electroanalytical properties of cytochrome *c* by direct electrochemistry on multi-walled carbon nanotubes incorporated with DNA biocomposite film

Jan-Wei Shie, Umasankar Yogeswaran, Shen-Ming Chen *

Department of Chemical Engineering and Biotechnology, National Taipei University of Technology, No. 1, Section 3, Chung-Hsiao East Road, Taipei 106, Taiwan, ROC

Received 9 August 2007; received in revised form 14 October 2007; accepted 15 October 2007
Available online 26 October 2007

Abstract

A novel conductive biocomposite film (MWCNTs–DNA–cyt *c*) which contains multi-walled carbon nanotubes (MWCNTs) along with the incorporation of DNA and cytochrome *c* (cyt *c*) has been synthesized on glassy carbon electrode (GCE), gold (Au), indium tin oxide (ITO) and screen printed carbon electrode (SPCE) by potentiostatic methods. The presence of both MWCNTs and DNA in the biocomposite film enhances the surface coverage concentration (Γ), increases the electron transfer rate constant (K_s) up to 21% and decreases the degradation of cyt *c* during the cycling. The biocomposite film also exhibits a promising enhanced electrocatalytic activity towards the reduction of halogen oxyanions and oxidation of biochemical compounds such as ascorbic acid and L-cysteine. The cyclic voltammetry has been used for the measurement of electroanalytical properties of analytes by means of biocomposite film modified GCEs. The sensitivity of MWCNTs–DNA–cyt *c* modified GCE possess higher values than the values obtained for DNA–cyt *c* film modified GCE. Further, the reduction potentials of halogen oxyanions E_{pc}, clearly shows that the activity of the biocomposite is dependent on the electronegativity of halogen oxyanions. Electrochemical quartz crystal microbalance studies revealed the enhancements in the functional properties of MWCNTs, DNA and cyt *c*. We have studied the surface morphology of the biocomposite films using scanning electron microscopy and atomic force microscopy, which revealed that DNA and cyt *c* have been incorporated on MWCNTs. Finally, the flow injection analysis has been used for the amperometric detection of analytes at MWCNTs–DNA–cyt *c* film modified SPCE.

Keywords: Multi-walled carbon nanotubes; Composite film; Modified electrodes; Electrocatalysis; Halogen oxyanions; Vitamin c; L-Cysteine

1. Introduction

Cytochrome *c* protein (cyt *c*) has received considerable importance in recent years in the field of electroanalytical chemistry because of its unique binding property with other protein redox partners. The direct electron transfer of cyt *c* was first observed by Bowden et al. [1,2] but in that observation, the cyt *c* showed transient response and short-life on the metal surfaces. These shortcomings can be explained as; firstly the cyt *c* molecules form irreversible adsorption blocks on the electrode surface, secondly the poisoning and deactivation of protein molecules unfold and then the adsorption of these occur on the bare electrodes [3–5]. Studies were carried out previously to enhance the electron transfer rate of cyt *c* on the metal electrodes. But, these too showed an apparent deactivation by oligomer formation on the electrode surface [6–8]. After that, in the following decades, an idea of using an electrode surface that was modified with some species having specific adsorption interaction to improve the electron transfer rate of cyt *c* had been proposed [9–12]. Not limited to these sorts of ideas, numerous other studies were also carried out on cyt *c* using solid state electrodes, oligomer and some polymers as promoters [13–15]. However, the results showed that the interaction and binding of cyt *c* to all those electrodes were weak. Recently, charge–transfer interactions have also been reported between cyt *c* and deoxyribonucleic acid (DNA) [16]. DNA molecule contains three constituents as, phosphate acid groups, basic groups, and sugar units. The basic groups are adenine, guanine, cytosine and thymine. The structure of the DNA consists of two molecular chains, in which one chain is tightly bound to the other to

* Corresponding author. Tel.: +886 2270 17147; fax: +886 2270 25238.
E-mail address: smchen78@ms15.hinet.net (S.-M. Chen).

0039-9140/$ – see front matter © 2007 Elsevier B.V. All rights reserved.
doi:10.1016/j.talanta.2007.10.034

form a double helix and they are held together by many hydrogen bonds. Further, DNA is classified as natural polymer. The direct electron transfer of heme proteins and horseradish peroxidase immobilized on DNA modified electrodes were used for sensor applications [17]. The interaction of DNA with metal proteins in the analysis of electroactive metal proteins, especially cyt *c* was also reported [18].

On the other hand, a wide variety of applications of matrices made of carbon nanotubes (CNTs) for the detection of bioorganic and inorganic compounds such as insulin, ascorbic acid, etc. were also already reported [19–22]. The rolled-up graphene sheets of carbon, i.e., CNTs, exhibits a π-conjugative structure with a highly hydrophobic surface. This property of the CNTs allows them to interact with some organic aromatic compounds through π–π electronic and hydrophobic interactions [23–25]. These interactions are used for preparing composite sandwiched films for electrocatalytic studies [26] and in the designing of nanodevices with the help of non-covalent adsorption of enzyme and proteins on the side walls of CNTs. This has resulted in a novel CNTs based nanostructures which contain biochemical units in them [27]. Some attempts were also made to prepare hydrophilic surface CNTs to overcome the dispersion problems in aqueous medium for bio-electrochemical applications [28]. Electrodes modified with composite films are widely used in capacitors, battery, fuel cells, chemical sensors and biosensors [29–31]. Even though the electrocatalytic activity of the CNTs with protein matrices individually showed good results; some properties like mechanical stability, sensitivity for different techniques and electrocatalysis for multiple compound detections are found to be poor.

Interestingly, the direct electron transfer between the cyt *c* and DNA modified electrode from aqueous solution and its catalytic activity towards different compounds have already been reported [18]. Further, the literature survey reveals that there were no previous attempts for the synthesis of biocomposite film composed of CNTs, DNA and cyt *c* for use in sensor applications. In this paper, we report about a novel biocomposite film (MWCNTs–DNA–cyt *c*) made of multi-walled carbon nanotubes (MWCNTs) which has been incorporated with DNA and cyt *c*. Its characterization and enhancement in functional properties, stability, peak current and electrocatalytic activity have also been reported along with its application in electrocatalysis of halogen oxyanions, ascorbic acid (AA) and L-cysteine (LC). Among these, the halogen oxyanions catalytic reductions at MWCNTs–DNA–cyt *c* biocomposite film are dependent on their electronegativity. The film formation processing involves the modification of glassy carbon electrode (GCE) with uniformly well dispersed MWCNTs and which is then modified with DNA. The modified MWCNTs–DNA GCE is then electrodeposited with cyt *c* from the neutral aqueous solution.

2. Experimental

2.1. Apparatus

Cyclic voltammetry (CV) were performed in an analytical system model CHI-611, CHI-400 and CHI-1205A potentiostat. A conventional three-electrode cell assembly consisting of an Ag/AgCl reference electrode and a Pt wire counter electrode were used for the electrochemical measurements. The working electrode was either an unmodified GCE or a GCE modified with the DNA–cyt *c* or MWCNTs–DNA–cyt *c* biocomposite films. In these experiments, all the potentials have been reported versus the Ag/AgCl reference electrode. The working electrode used for the EQCM measurements was an 8 MHz AT-cut quartz crystal coated with gold electrode. The diameter of the quartz crystal was 13.7 mm; the gold electrode diameter was 5 mm. The flow injection analysis (FIA) of the analytes at screen printed carbon electrode (SPCE) was done using Alltech 426 HPLC pump containing an electrochemical cell. The morphological characterizations of the films were examined by means of SEM (Hitachi S-3000H) and atomic force microscopy (AFM) (Being Nano-Instruments CSPM4000). All the measurements were carried out at 25 °C ± 2.

2.2. Materials

Cytochrome *c* (cyt *c*), multi-walled carbon nanotubes (MWCNTs OD = 10–20 nm, ID = 2–10 nm and length = 0.5–200 μm), DNA, potassium hydroxide, L-cysteine and ascorbic acid were obtained from Aldrich and Sigma–Aldrich, KIO_3 and $KClO_3$ from Osaka and $KBrO_3$ from Nakarai were used as received. All other chemicals used were of analytical grade. The preparation of aqueous solution was done with twice distilled deionized water. Solutions were deoxygenated by purging with prepurified nitrogen gas. Buffer solutions were prepared from H_2SO_4 and 2-amino-2-hydroxymethyl-1,3-propanediol (0.1 M TRIS buffer) for the pH 1.0 and 8.4, respectively.

2.3. Preparation of MWCNTs and MWCNTs–DNA–cyt c modified electrodes

There was an important challenge in the preparation of MWCNTs. Because of its hydrophobic nature, it was difficult to disperse it in any aqueous solution to get a homogeneous mixture. Briefly, the hydrophobic nature of the MWCNTs was converted in to hydrophilic nature by following the previous studies [28]. This was done by weighing 10 mg of MWCNTs and 200 mg of potassium hydroxide in to a ruby mortar and grained together for 2 h at room temperature. Then the reaction mixture was dissolved in 10 ml of double distilled deionized water and it was precipitated many times in to methanol for the removal of potassium hydroxide. Thus obtained MWCNTs in 10 ml water was ultrasonicated for 6 h to get a uniform dispersion. This functionalization process of MWCNTs was done to get a hydrophilic nature by which, the MWCNTs can be homogeneously dispersed in water. This process not only converts MWCNTs to hydrophilic nature but this helps to breakdown larger bundles of MWCNTs in to smaller ones also. This process was confirmed using SEM, which is not shown in the figures. Then a homogenous 0.45 mg ml^{-1} concentration of DNA solution was prepared in double distilled deionized water.

Before starting each experiment, the GCEs were polished by a BAS polishing kit with 0.05 μm alumina slurry, rinsed and then

ultrasonicated in double distilled deionized water. The GCEs studied were uniformly coated with 5.8 μg cm^{-2} of MWCNTs then dried, and then coated with 4.4 μg cm^{-2} of DNA and again dried at 35 °C. The concentrations of homogeneously dispersed MWCNTs and DNA were exactly measured using micro-syringe. The electrochemical deposition of cyt *c* was performed from 2×10^{-4} M cyt *c* in pH 8.4 TRIS buffer aqueous solution by consecutive CV over a suitable potential region of −0.2 to 0.3 V. Then, the modified MWCNTs–DNA–cyt *c* electrode was carefully washed with double distilled deionized water. The concentrations of homogeneously dispersed MWCNTs and DNA were exactly measured using micro-syringe. For a detailed comparison of electrocatalysis reactions, we studied different types of modified electrodes such as DNA–cyt *c*, MWCNTs–cyt *c* and MWCNTs–DNA–cyt *c*. In all these studies, the electrodes were first modified by MWCNTs, DNA and then electrodeposited with cyt *c*. These characterization studies were done to reveal the obvious necessity for the presence of MWCNTs in the DNA–cyt *c* biocomposite film.

3. Results and discussions

3.1. Electrochemical synthesis of MWCNTs–DNA–cyt c biocomposite film and its characterization

The electrochemical deposition of cyt *c* (2×10^{-4} M) on MWCNTs–DNA modified GCE present in pH 8.4 TRIS buffer solution has been performed by consecutive CV for the preparation of MWCNTs–DNA–cyt *c* biocomposite film. The suitable potential range for cyt *c* deposition has been found to be −0.2 to 0.3 V (see ESI[1]). In the following experiments, each newly prepared biocomposite film on GCE has been washed carefully in deionized water to remove the loosely bounded cyt *c* on the modified GCE. It was then transferred to pH 8.4 of 0.1 M TRIS buffer or pH 1.0 aqueous solutions for the other electrochemical characterizations. These optimized pH solutions have been chosen to maintain the higher stability of the biocomposite film. Fig. 1(A) represents the electrochemical signal of cyt *c* at 20 mV s^{-1} on (a′) DNA modified GCE with a $Fe^{III/II}$ redox couple corresponding to the redox reaction of cyt *c* with the formal potential $E^{0\prime}$ = 8.95 mV versus Ag/AgCl in TRIS buffer solution, and no redox peak in (b′) show that there is no direct electron transfer of cyt *c* occurred at MWCNTs modified GCE, whereas in (c′) similar redox couple of cyt *c* show higher peak current at MWCNTs–DNA modified GCEs with the formal potential of $E^{0\prime}$ = −31.55 mV. When comparing with the formal potentials of cyt *c*, in both the cases (a′) and (c′), there is a shift in $E^{0\prime}$ towards lower positive potential of about 40.5 mV in the presence of MWCNTs. Also, there is a decrease in ΔE value of about 7.9 mV in the presence of MWCNTs. This is because of the high reversibility of cyt *c* in the presence of MWCNTs–DNA. The higher ΔE value for cyt *c* at DNA modified GCE could be the cause of an irreversible adsorption of cyt *c* on the modified electrode [18]. Further, comparing (b′) with the other two CVs (a′ and c′) in the same figure reveals the importance of DNA on the biocomposite film, where GCE modified with only MWCNTs has no active redox couple growth for cyt *c* (ESI see Footnote 1). The biocomposite film formation and the interactions between MWCNTs, DNA and cyt *c* can be cleaved in to two steps. The foremost step is the attachment of DNA on MWCNTs, this could happen in two ways, either by the attachment of amine groups present in DNA with that of carboxyl groups of modified MWCNTs or by the attachment of DNA on the sidewalls of MWCNTs by hydrophobic interactions [32]. The second step is the attachment of cyt *c* on the DNA. The immobilization of cyt *c* on DNA and the interaction between both of these compounds can be explained as the electrostatic attraction between the positively charged lysine (pK_a = 10.8) $-NH_3^+$ group or the other positively charged groups such as Fe^{2+} and Fe^{3+} in cyt *c* with that of the negatively charged phosphates of the DNA backbone [18,32]. Scheme 1 shows the possible interactions between MWCNTs, DNA and cyt *c*. From these CVs in Fig. 1(A), the surface cover-

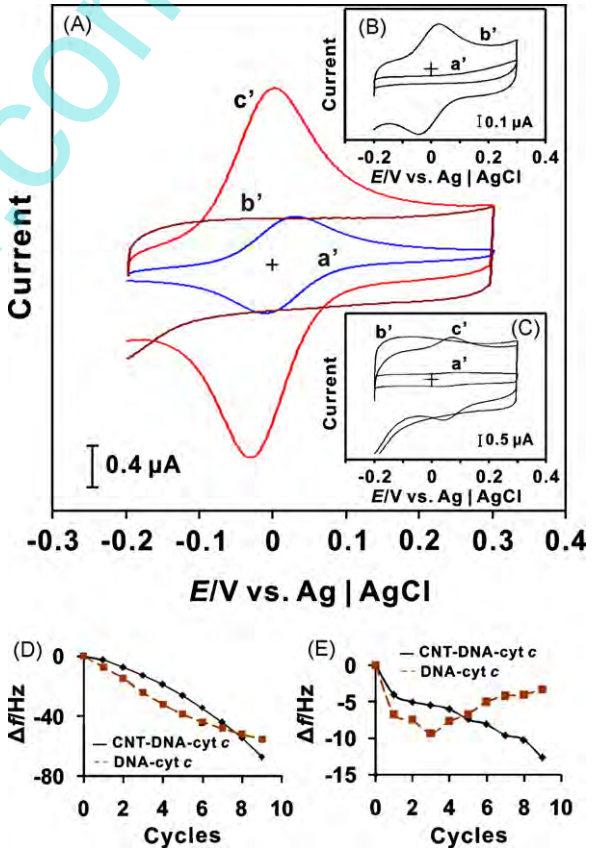

Fig. 1. (A) Comparison of CVs of (a′) DNA–cyt *c*, (b′) MWCNTs–cyt *c* and (c′) MWCNTs–DNA–cyt *c* biocomposite films at GCE in 0.1 M pH 8.4 TRIS buffer, scan rate at 20 mV s^{-1}, the redox couples in these CVs represents ($Fe^{III/II}$) reactions of cyt *c*. (B) CVs of Au modified from (a′) DNA–cyt *c* and (b′) MWCNTs–DNA–cyt *c* at similar conditions to that of GCE. (C) CVs of ITO modified from (a′) DNA–cyt *c*, (b′) MWCNTs–cyt *c* and (c′) MWCNTs–DNA–cyt *c* at similar conditions to that of GCE. From these CVs, the peak current and the calculated values (Table 1) reveals that the increase in Γ of cyt *c* has been taken place in presence of DNA and MWCNTs at all the electrodes. (C) Plot of frequency change in EQCM vs. scan cycles and (D) every cycle frequency change vs. scan cycles for both the films. These results show the biocomposite is a stabilized one and it is deposited homogeneously.

[1] Electronic Supplementary Information (ESI) available.

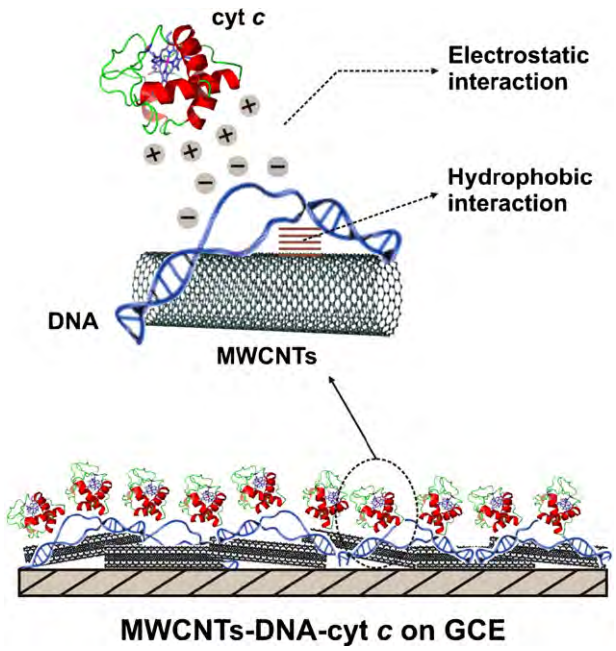

Scheme 1. Possible interaction between MWCNTs, DNA and cyt *c* for the formation of MWCNTs–DNA–cyt *c* biocomposite film modified electrodes.

age concentration (Γ) values have been calculated and are given in Table 1. In this calculation, the charge involved in the reaction (Q) has been obtained from CVs and it has been applied in the equation $\Gamma = Q/nFA$, where, the number of electron transfer involved in the cyt *c* redox reaction is assumed as two (one electron for each heme group) [18]. These values indicate that the presence of MWCNTs increased the surface area of the electrode, which in turn has increased the Γ of cyt *c*. For comparison, the Γ values at other modified electrodes from the literature have also been provided in the same table, and these values reveal that the MWCNTs–DNA at GCE enhances Γ of cyt *c* than the other modified electrodes.

Table 1
Surface coverage concentrations (Γ) of cyt *c* at different types of modified electrodes

Electrode type	Modified film	Γ (mol cm^{-2})
GCE[a]	DNA–cyt *c*	6.11×10^{-12}
	MWCNTs–DNA–cyt *c*	2.34×10^{-11}
Au[a]	DNA–cyt *c*	No peak
	MWCNTs–DNA–cyt *c*	6.72×10^{-12}
ITO[a]	DNA–cyt *c*	2.41×10^{-12}
	MWCNTs–cyt *c*	No peak
	MWCNTs–DNA–cyt *c*	1.50×10^{-11}
Mixed SAMs of MES/MEL[b] [42]		7.70×10^{-12}
SAMs of (T-COOH)/(T-NH$_2$)[c] [43]		9.20×10^{-12}
Fullerene [44]		1.70×10^{-11}
N-Butylpyridinium tetrafluoroborate [45]		1.57×10^{-11}
Sulfonated polyaniline nano-networks [46]		9.80×10^{-12}
Planar ITO [47]		9.50×10^{-12}
SAM of ω-carboxylalkanethiols [48]		1.19×10^{-12}

[a] Studied using CV technique in 0.1 M TRIS buffer aqueous solution (pH 8.4).
[b] MES/MEL is 2-mercaptoethanesulfonate/2-mercaptoethanol.
[c] (T-COOH)/(T-NH$_2$) is thioctic acid/thioctic amide.

Gold and ITO electrodes have also been used to characterize the biocomposite films in pH 8.4 TRIS buffer aqueous solution. Fig. 1(B) represents the redox peaks of cyt *c* on DNA modified Au electrodes in (a′) absence and (b′) presence of MWCNTs, where there is no peak for cyt *c* on DNA modified Au. This obviously shows that there is no occurrence of direct electron transfer on DNA modified Au as reported previously [18]. Similarly, Fig. 1(C) represents the redox peaks of cyt *c* on ITO modified electrodes in (a′) presence of DNA, (b′) presence of MWCNTs and (c′) presence of both DNA and MWCNTs. These results too reveal the importance of the presence of DNA and MWCNTs in the biocomposite films. This condition enhances the electron transfer on different electrodes which in turn widens their use in the sensor based applications. However, comparison of data in Table 1 shows that Γ of cyt *c* is lower on MWCNTs–DNA modified Au than that of MWCNTs–DNA modified GCE. The percentage of degraded Γ of cyt *c* on MWCNTs–DNA modified Au on comparing with GCE has been calculated as 249%. The electrochemical quartz crystal microbalance (EQCM) experiments have been carried out by modifying the gold in electrochemical quartz crystal with uniformly coated MWCNTs and DNA, which has been dried at 35 °C (ESI see Footnote 1). From the frequency change, the change in the mass of biocomposite film at the quartz crystal has been calculated by the Sauerbrey equation, however 1 Hz frequency change is equivalent to 1.4 ng of mass change [33,34]. The mass change during cyt *c* incorporation on the DNA modified and MWCNTs–DNA modified Au for total cycles has been found to be 77.85 and 93.92 ng cm^{-2}, respectively, which are consistent with that of the Γ of cyt *c* values. However, in both cases because of the poor direct electron transfer, the redox peak currents are very low. Fig. 1(C) indicates the variation of frequency change with the increase of scan cycles and Fig. 1(D) indicates every cycle frequency change with the increase of the scan cycles. From these plots, it is clear that there has an unstable deposition of cyt *c* on the DNA modified Au when compared with the MWCNTs–DNA modified Au. Up to six cycles the cyt *c* deposition rate is higher in DNA modified Au than that of MWCNTs–DNA modified Au, however in later stages the rate of deposition on DNA modified Au has been drastically reduced. This proves that the deposition of cyt *c* on MWCNTs–DNA biocomposite film is more stabilized and more homogeneous than on the other modified electrodes. Similar previous studies on CNTs biocomposite have also shown the necessity of the CNTs for improving the functional properties such as orientation, enhanced electron transport, high capacitance, etc. [35,36].

3.2. Electrochemical and morphological characterization of MWCNTs–DNA–cyt c biocomposite film

The CVs of MWCNTs–DNA–cyt *c* biocomposite film on GCE in pH 8.4 TRIS buffer solution at different scan rates (ESI see Footnote 1) demonstrated that the redox process is not controlled by diffusion up to 200 mV s^{-1}. Further investigation reveals that, the separation between anodic and cathodic peak currents for both the films increased as the scan rate

increased up to 2.0 V s^{-1} (CVs not shown). However, in Fig. 2(A) the separation between the anodic and cathodic peak of MWCNTs–DNA–cyt *c* is lower than DNA–cyt *c*, which shows MWCNTs–DNA–cyt *c* posses faster electron transfer rate than DNA–cyt *c* film. Also, the peak to peak potential separation ΔE_p for MWCNTs–DNA–cyt *c* is <200 mV below 1.52 V s^{-1} scan rate, but DNA–cyt *c* shows $\Delta E_p > 200$ mV even for 1.36 V s^{-1}. From the slope values in Fig. 2(B), by assuming the value of $\alpha \approx 0.5$, the electron transfer rate constant has been calculated based on Laviron theory [37] is $K_s \approx 0.89\ s^{-1}$ for MWCNTs–DNA–cyt *c* and 0.73 s^{-1} for DNA–cyt *c*. From these

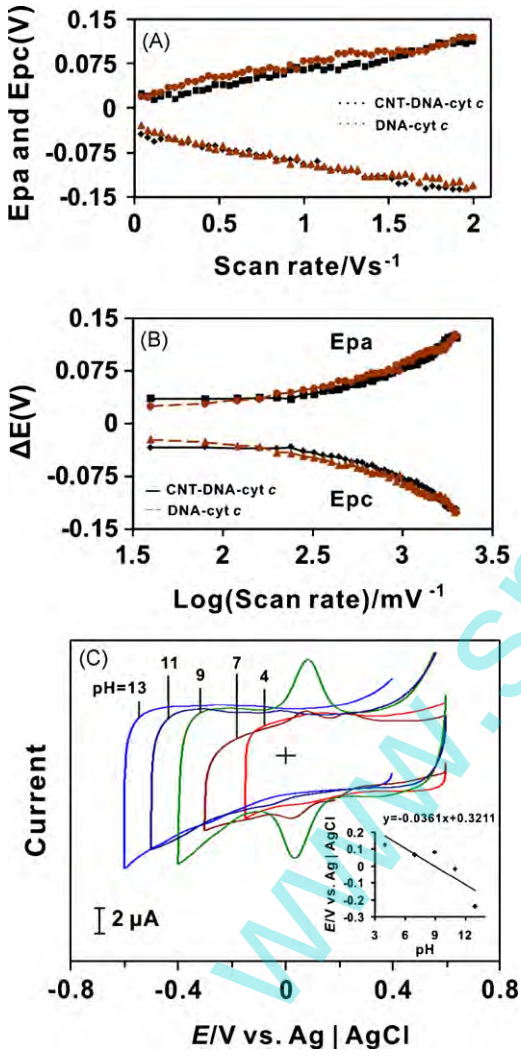

Fig. 2. (A) Shows the plot of E_{pa} and E_{pc} vs. different scan rate (0.02–2 V s^{-1}) for both DNA–cyt *c* and MWCNTs–DNA–cyt *c* biocomposite films present in 0.1 M pH 8.4 TRIS buffer. From this result, it is clear that the electron transfer rate is roughly higher for MWCNTs–DNA–cyt *c* biocomposite film when compared with DNA–cyt *c* film. (B) Shows a plot of ΔE vs. log of scan rate for both the films, from the slope values, α and K_s are calculated, which shows a higher K_s value for MWCNTs–DNA–cyt *c* biocomposite film when compared with DNA–cyt *c*. In all the curves the brown dotted line and the black continuous line represents DNA–cyt *c* and MWCNTs–DNA–cyt *c*, respectively. (C) CVs of the MWCNTs–DNA–cyt *c* biocomposite film synthesized at similar conditions and transferred to various pH solutions; scan rate: 100 mV s^{-1}. The inset in (C) shows the formal potential vs. pH (4–13), the slope −36 mV/pH is almost nearer to Nernstian equation for 2 electron and 1 proton transfer.

K_s values the increase in the ability of electron transfer between the electrode surface and the cyt *c* in presence of MWCNTs has been calculated and it is found to be ≈21%. These results too show that, there has been an enhancement in functional properties of the biocomposite film at lower scan rates in presence of both DNA and MWCNTs.

Fig. 2(C) shows the CVs of MWCNTs–DNA–cyt *c* on GCE at various pH aqueous buffers solutions in which the cyt *c* is absent. In these experiments, the GCE has been modified with cyt *c* using pH 8.4 TRIS buffer solution, and then it has been washed with deionized water and then transferred to various pH aqueous buffer solutions for CV measurements. These CV results show that the film is stable in the pH range between 7 and 11 and the E_{pa} and E_{pc} values depends on the pH value of the buffer solution. In other pH solutions, the $Fe^{III/II}$ redox couple of cyt *c* is not clearly visible. In detail, the CVs of the biocomposite film in pH 4, 7 and 9 shows that the cyt *c* is stable in these pH solutions. However at pH 11, the partial denaturation of cyt *c* reduces the peak current of $Fe^{III/II}$ redox couple. Further, it is obvious that the broad peak with low peak current of $Fe^{III/II}$ redox couple in pH 13 is because of the total denaturation of cyt *c*. The inset in Fig. 2(C) shows the formal potential of MWCNTs–DNA–cyt *c* plotted over a pH range of 4–13. The response shows a slope of −36 mV/pH, which is close to that given by the Nernstian equation for two electron one proton transfer [38]. The enhanced stability of the cyt *c* in presence of DNA and MWCNTs has been studied (ESI see Footnote 1) and the percentage of degradation [39] of MWCNTs–DNA–cyt *c* and DNA–cyt *c* is calculated. The amount of degradation after 120 min cycling for MWCNTs–DNA–cyt *c* and DNA–cyt *c* is less than 16.39% and 36.37%, respectively and the percentage of decrease in degradation of cyt *c* in presence of MWCNTs is about 19.99% for 120 min cycling. Similar enhancements in the biocomposite properties in presence of CNTs have been already reported in the literature [35,36].

Further, four different films; cyt *c*, DNA–cyt *c*, MWCNTs–cyt *c* and MWCNTs–DNA–cyt *c* have been prepared on the indium tin oxide (ITO) with similar conditions and similar potential as that of GCE and were characterized using SEM. From Fig. 3, it is significant that there are morphological differences between all these four films. All the four film images have been measured at the same resolution of about ×2 k. It is a well known fact that the prolonged exposure to the electron beam will damage the cyt *c* films, so an at most care was taken to measure these images. The top views of nanostructures Fig. 3(A) on the ITO electrode surface show white patches of cyt *c* deposited on this electrode. When comparing this with Fig. 3(B)–(D) shows that the deposition of cyt *c* has taken place on both DNA modified and MWCNTs modified ITOs, respectively. However as discussed earlier, there is no redox couples observed for MWCNTs–cyt *c*, which shows the importance of DNA, which enhances the electron transfer for $Fe^{III/II}$ redox reaction in cyt *c*. The MWCNTs–DNA–cyt *c* biocomposite film in Fig. 3(D) reveals that the DNA had covered the entire MWCNTs to form MWCNTs–DNA biocomposite and then the cyt *c* has been deposited on the MWCNTs–DNA modified ITO. The dotted

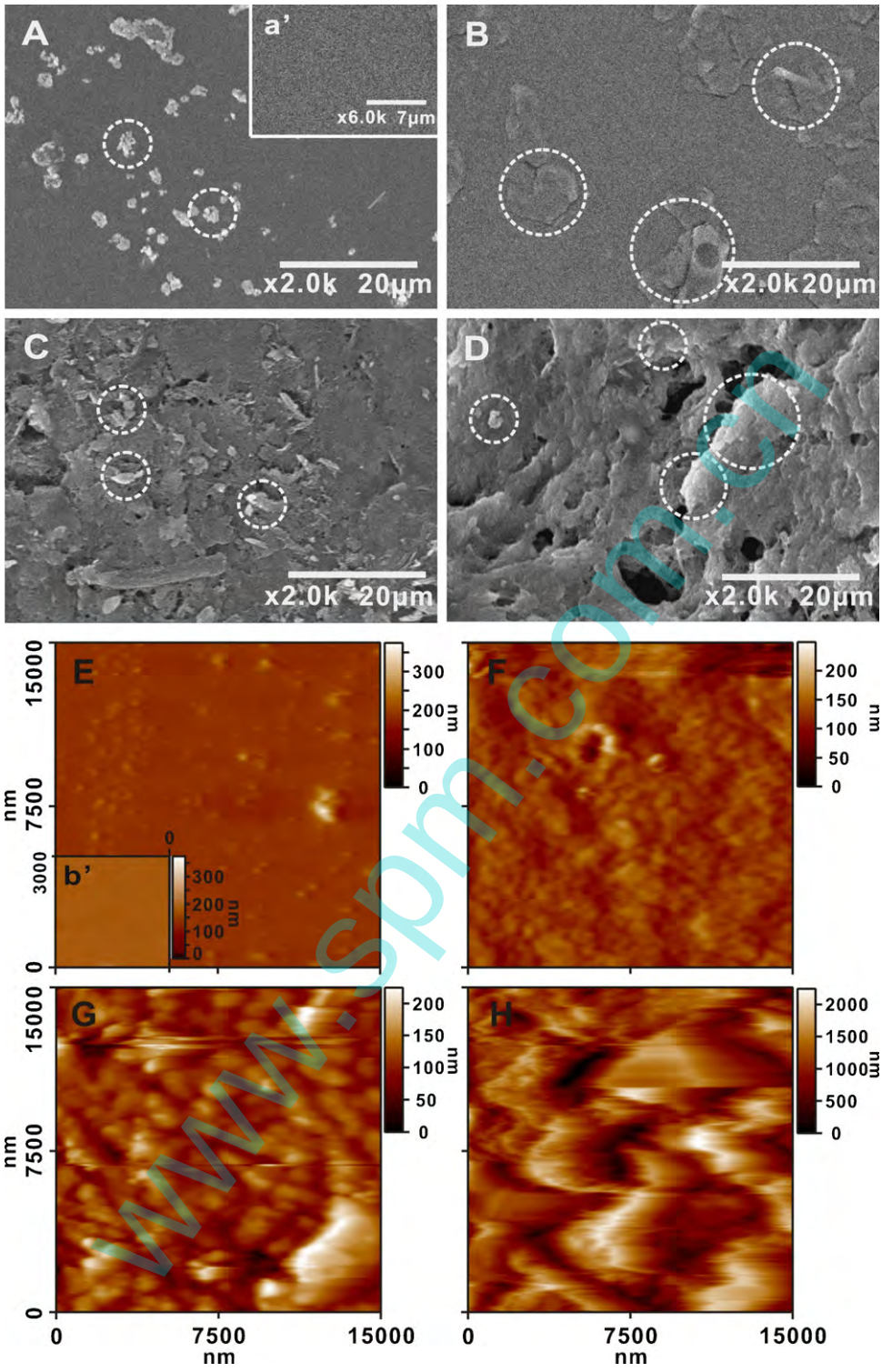

Fig. 3. SEM images of (A) cyt *c*, (B) DNA–cyt *c*, (C) MWCNTs–cyt *c* and (D) MWCNTs–DNA–cyt *c* biocomposite films. The white dotted circles represent the incorporation of cyt *c* on the unmodified and modified electrodes. AFM topography images of (E) cyt *c*, (F) DNA–cyt *c*, (G) MWCNTs–cyt *c* and (H) MWCNTs–DNA–cyt *c* biocomposite films. It is obvious that the observed morphological structure is similar to that of the structures obtained in SEM. (a′) and (b′) are the SEM and AFM images of bare ITO. Comparing all the figures it is obvious that the formation of biocomposite film in (D) and (H).

circles in all the four figures reveal that the deposition of cyt *c* occurred on the unmodified or modified ITOs. The same modified ITO electrodes have been used to measure the AFM topography images of (E) cyt *c*, (F) DNA–cyt *c*, (G) MWCNTs–cyt *c* and (H) MWCNTs–DNA–cyt *c*. In all these cases the observed morphological structure is similar to that of SEM. Further, for comparison, the SEM and AFM images of the bare ITO is shown in (a′) and (b′), respectively. These SEM and AFM results show the obvious formation of MWCNTs–DNA–cyt *c* biocomposite film.

3.3. Electroanalytical response of halogen oxyanions at MWCNTs–DNA–cyt c biocomposite film

The MWCNTs–DNA–cyt *c* biocomposite films have been synthesized on GCE at similar conditions as given in Section 2. Then, the modified biocomposite films have been washed carefully in deionized water and transferred to pH 1.0 H_2SO_4 aqueous solutions for studying the electrocatalysis of halogen oxyanions such as IO_3^-, BrO_3^- and ClO_3^-. This pH has been chosen as the most suitable one, as it is a well known fact that the reduction of halogen oxyanions is dependent on pH of the reaction medium [40]. All the CVs have been recorded at the constant time interval of 1 min with nitrogen purging before the start of each experiments. Generally in all the sections of Fig. 4, a′ represents bare GCE, b′ represents DNA–cyt *c* film and c′ represents MWCNTs–cyt *c* film modified GCEs. Fig. 4(A)–(C) shows the electrocatalytic reduction of IO_3^-, BrO_3^- and ClO_3^- at MWCNTs–DNA–cyt *c* biocomposite films, respectively at 20 mV s^{-1}. The CVs for MWCNTs–DNA–cyt *c* exhibit a reversible redox couple for cyt *c* ($Fe^{III/II}$) in the absence of the analytes, and upon addition of analytes, a new growth in the reduction peak of analytes appeared at $E_{pc} = -120$ mV for IO_3^-, $E_{pc} = -144$ mV for BrO_3^- and $E_{pc} = -163$ mV for ClO_3^-. These peak currents show that electrocatalytic reduction of all the three analytes took place at cyt *c* (Fe^{III}). Based on these results, the reaction between the analytes and the cyt *c* catalyst can be explained by the following Eqs. (1)–(3):

$$\text{cyt } c\,(Fe^{III}) + IO_3^- \rightarrow \text{cyt } c\,(Fe^{II}) + I^- \quad (1)$$

$$\text{cyt } c\,(Fe^{III}) + 2BrO_3^- \rightarrow \text{cyt } c\,(Fe^{II}) + Br_2 \quad (2)$$

$$\text{cyt } c\,(Fe^{III}) + 2ClO_3^- \rightarrow \text{cyt } c\,(Fe^{II}) + Cl_2 \quad (3)$$

An increase in concentration of analytes simultaneously produced a linear increase in the reduction peak currents of the analytes with good film stability as shown in the insets in Fig. 4(A)–(C). The cathodic peak currents are linear with the concentration of IO_3^- in the range of 5–15 μM. Similarly, for BrO_3^- and ClO_3^- it is in the range of 40–120 μM and 0.3–0.9 mM, respectively. It is obvious that the MWCNTs–DNA–cyt *c* shows higher electrocatalysis for IO_3^- and BrO_3^- when compared to all the other films. More specifically, the enhanced electrocatalysis of MWCNTs–DNA–cyt *c* can be explained in terms of higher peak current than that of MWCNTs–cyt *c*; and the both lower in overpotential and higher peak current than that of DNA–cyt *c*. Similarly, ClO_3^- shows higher electrocatalysis at MWCNTs–DNA–cyt *c* than all other films in terms of both lower in overpotential and higher peak current. These results can be observed from the I_{pa} and E_{pa} values in Table 2. Where, the increase in current and lower in overpotential, both are considered as the cause for the enhancement of electrocatalysis [41]. From the slopes of the linear calibration curves, the sensitivities of DNA–cyt *c* and MWCNTs–DNA–cyt *c* biocomposite modified GCEs and their correlation coefficient have been calculated and are given in Table 3. It is obvious that the sensitivity of MWCNTs–DNA–cyt *c* is high for all the three analytes when compared with DNA–cyt *c* modified GCEs. The shift towards negative potential in the E_{pa} values of IO_3^-, BrO_3^- and ClO_3^- clearly show that the electrocatalysis of halogen oxyanions at MWCNTs–DNA–cyt *c* biocomposite film is dependent on the analytes electronegativity. The overall view of these results, clearly reveal that MWCNTs–DNA–cyt *c* biocomposite film is efficient for halogen oxyanions detection.

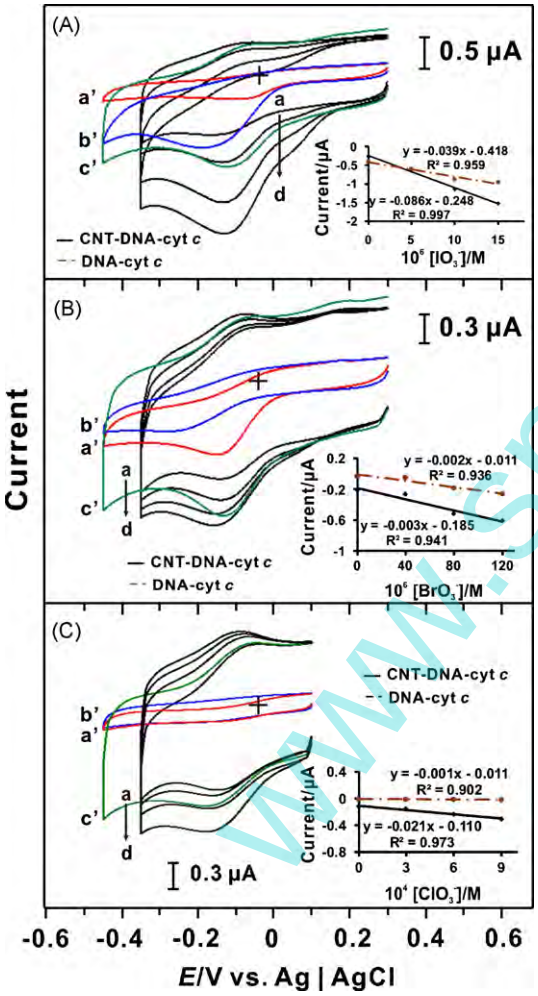

Fig. 4. (A) CVs of MWCNTs–DNA–cyt *c* biocomposite film in pH 1.0 H_2SO_4 aqueous solution with various concentrations of IO_3^- = (a) 0.0 M; (b) 5×10^{-6} M; (c) 1×10^{-5} M and (d) 1.5×10^{-5} M, where (a′), (b′) and (c′) in all the sections in figures represents bare, DNA–cyt *c* and MWCNTs–cyt *c* modified GCEs, respectively at the highest concentration of the analytes; scan rate: 20 mV s^{-1}. Similarly, (B) represents [BrO_3^-] = (a) 0.0 M; (b) 4×10^{-5} M; (c) 8×10^{-5} M and (d) 1.2×10^{-4} M. Similarly, (C) represents [ClO_3^-] = (a) 0.0 M; (b) 3×10^{-4} M; (c) 6×10^{-4} M and (d) 9×10^{-4} M. The insets in (A), (B) and (C) show the plot of current vs. different concentration of analytes, respectively at biocomposite films.

3.4. Electroanalytical response of ascorbic acid and L-cysteine at MWCNTs–DNA–cyt c biocomposite film

Fig. 5(A) and (B) shows the electrocatalytic oxidation of ascorbic acid (AA) and L-cysteine (LC), respectively. The electrolyte used for the electrocatalytic reactions was pH 8.4 TRIS aqueous buffer solution. In these studies, similar electrolyte has

Table 2
Comparison of E_{pa} and I_{pa} of analytes in electrocatalysis reactions using CV technique at different types of modified electrodes in pH 8.4 TRIS buffer solution

Analytes	Reaction type	pH	E_p (mV)			I_p (μA)		
			cyt c[a]	cyt c[b]	cyt c[c]	cyt c[a]	cyt c[b]	cyt c[c]
IO_3^-	Reduction	1.0	−190.0	−118.0	−120.0	−0.96	−0.58	−1.57
BrO_3^-	Reduction	1.0	−262.0	−125.0	−144.0	−0.33	−0.61	−0.76
ClO_3^-	Reduction	1.0	−181.1	−182.0	−163.0	−0.02	−0.29	−0.36
AA	Oxidation	8.4	79.0	−16.0	6.0	0.02	1.00	1.47
LC	Oxidation	8.4	61.0	70.0	58.0	0.01	0.32	0.89

[a] DNA modified GCE.
[b] MWCNTs modified GCE.
[c] MWCNTs–DNA modified GCE.

been used for both MWCNTs–DNA–cyt c biocomposite film preparation and the electrocatalytic studies. The CVs have been recorded at the constant time interval of 1 min with nitrogen purging before the start of each experiments. The scan rate used for electrocatalysis was 20 mV s^{-1}. In all the sections of Fig. 5, a′ represents bare GCE, b′ represents DNA–cyt c film and c′ represents MWCNTs–cyt c film modified GCEs. The CVs of the MWCNTs–DNA–cyt c in Fig. 5(A) and (B) exhibits a reversible redox couple for cyt c ($Fe^{III/II}$) in the absence of the analytes, upon addition of analytes, a new growth in the oxidation peak of analytes appeared at E_{pa} = 6 mV for AA and E_{pa} = 58 mV for LC. These peak currents show that electrocatalytic oxidation of both the analytes took place at cyt c (Fe^{II}). The interaction between the film and the analytes can be explained by the following equations, where (4) is for AA and (5) for LC [18]:

$$2\,\text{cyt}\,c\,(Fe^{II}) + \text{AA} \rightarrow 2\,\text{cyt}\,c\,(Fe^{III}) + \text{DHA} \quad (4)$$

$$\text{cyt}\,c\,(Fe^{II}) + 2\,CyS^- \rightarrow \text{cyt}\,c\,(Fe^{III}) + \text{CySSCy} \quad (5)$$

where DHA is dehydroascorbic acid (oxidized product of AA), CyS^- is L-cysteine and CySSCy is L-cysteine (L-cysteine's oxidized product). During the electrocatalysis experiments, an increase in concentration of analytes simultaneously produced a linear increase in the oxidation peak currents of the analytes with good film stability as shown in the insets in Fig. 5(A) and (B). The anodic peak currents are linear with the concentration of AA in the range of 0.1–0.4 mM. Similarly, for LC it is in the range of 0.6–2.1 mM. It is obvious that the MWCNTs–DNA–cyt c show higher electrocatalysis for both the analytes when compared to that of all other modified GECs, as we can observe it from the I_{pa} and E_{pa} values in Table 2. Further, the values in the same table reveal that there is no obvious peak for both the analytes at DNA–cyt c film. From the slopes of the linear calibration curves the sensitivity of the DNA–cyt c and MWCNTs–DNA–cyt c biocomposite modified GCEs and their correlation coefficient have been calculated and are given in Table 3. It is clear that, the sensitivity of MWCNTs–DNA–cyt c is higher for both the analytes and there is no electrocatalysis reaction at DNA–cyt c modified GCEs. These results clearly show that, the MWCNTs–DNA–cyt c biocomposite film can be efficiently used for the detection of AA and LC.

Table 3
Sensitivities and correlation coefficients of different modified electrodes for various analytes in CV technique

Analytes	Reaction type	Sensitivity (μA mM^{-1} cm^{-2}) [correlation coefficient]	
		DNA–cyt c	MWCNTs–DNA–cyt c
IO_3^-	Reduction	−37.6 [0.959]	−83.0 [0.997]
BrO_3^-	Reduction	−1.9 [0.936]	−2.9 [0.941]
ClO_3^-	Reduction	−1.0 [0.902]	−20.3 [0.973]
AA	Oxidation	−0.12 [0.952][a]	2.17 [0.988]
LC	Oxidation	−0.012 [0.673][a]	0.177 [0.875]

[a] The values indicate the instability and no electrocatalysis reaction at the film.

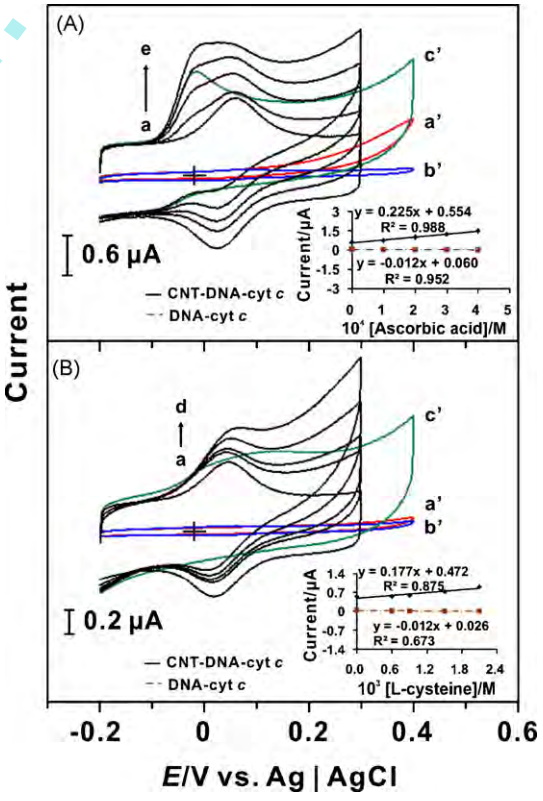

Fig. 5. (A) CVs of MWCNTs–DNA–cyt c biocomposite film in 0.1 M pH 8.4 TRIS buffer with five different concentrations of [AA] = (a) 0.0 M; (b) 1×10^{-4} M; (c) 2×10^{-4} M; (d) 3×10^{-4} M and (e) 4×10^{-4} M; scan rate: 20 mV s^{-1}. Similarly, (B) represents [LC] = (a) 0.0 M; (b) 6×10^{-4} M; (c) 9×10^{-4} M; (d) 1.5×10^{-3} M and (e) 2.1×10^{-3} M. The insets in (A) and (B) show the plot of current vs. different concentration of analytes, respectively at biocomposite films.

3.5. Flow injection analysis of the analytes at MWCNTs–DNA–cyt c biocomposite film

The MWCNTs–DNA–cyt *c* biocomposite films have been synthesized on SPCE at similar conditions to that of GCE. Then, the modified electrodes have been washed carefully in deionized water and used for the FIA of halogen oxyanions such as (A) IO_3^-, (B) BrO_3^- and (C) ClO_3^- as shown in Fig. 6. The carrier stream used was pH 1.0 H_2SO_4 aqueous solution with the flow rate of 0.03 ml s^{-1} and the volume of analytes injected at each cycle was 10 μl at the time interval of 50 s. All parts in Fig. 6 are the successive addition of analytes in the concentration range from 10 μM to 10 mM at the potential of −120.0 mV for IO_3^-, −144.0 mV for BrO_3^- and −163.0 mV for ClO_3^-, these are the optimized potentials obtained from CV studies. The rapid amperometric response of the MWCNTs–DNA–cyt *c* biocomposite film is proportional to the respective analytes concentration. After plotting these results, the slope obtained from the insets in Fig. 6

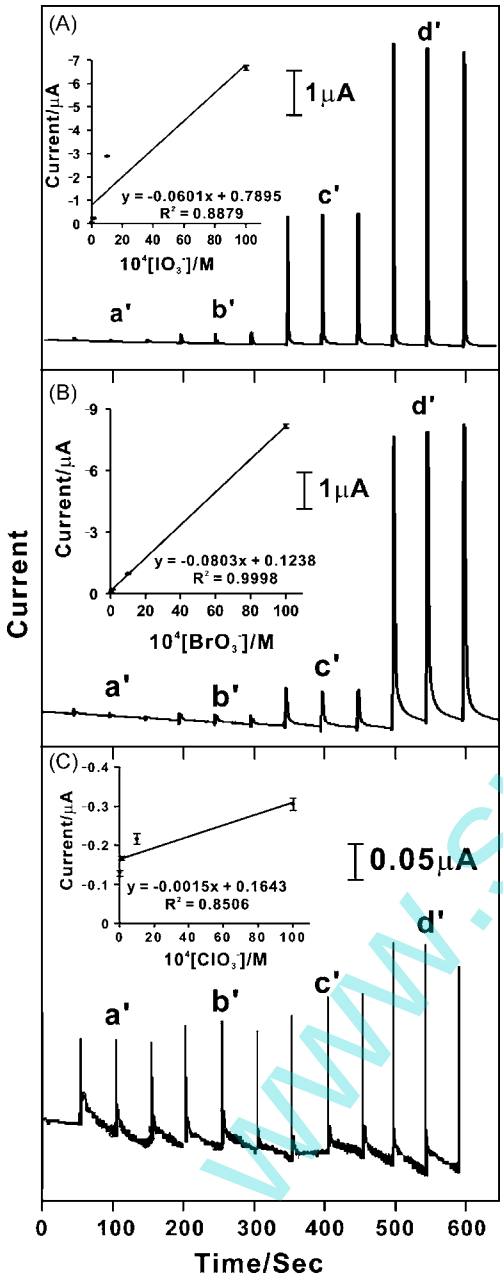

Fig. 6. (A) Flow-amperometric detection of halogen oxyanions at MWCNTs–DNA–cyt *c* biocomposite film present in pH 1.0 H_2SO_4 aqueous solution with four different concentrations of IO_3^- = (a′) 1×10^{-5} M; (b′) 1×10^{-4} M; (c′) 1×10^{-3} M and (d′) 1×10^{-2} M; potential = −120.0 mV. Similarly, (B) represents $[BrO_3^-]$ = (a′) 1×10^{-5} M; (b′) 1×10^{-4} M; (c′) 1×10^{-3} M and (d′) 1×10^{-2} M; potential = −144.0 mV. Similarly, (C) represents $[ClO_3^-]$ = (a′) 1×10^{-5} M; (b′) 1×10^{-4} M; (c′) 1×10^{-3} M and (d′) 1×10^{-2} M; potential = −163.0 mV. In all these three experiments the carrier stream used was pH 1.0 H_2SO_4 aqueous solution; flow rate = 0.03 ml s^{-1} and injected volume = 10 μl. The insets in (A), (B) and (C) show the plot of current vs. different concentration of analytes, respectively at MWCNTs–DNA–cyt *c* biocomposite films.

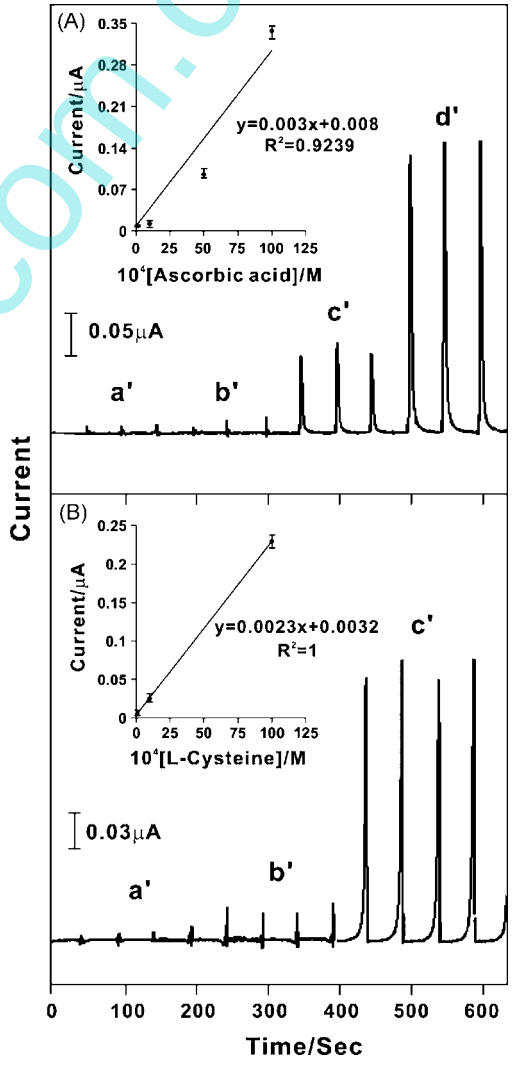

Fig. 7. (A) Flow-amperometric detection of AA and LC at MWCNTs–DNA–cyt *c* biocomposite film present in 0.1 M pH 8.4 TRIS buffer with four different concentrations of AA = (a′) 1×10^{-5} M; (b′) 1×10^{-4} M; (c′) 1×10^{-3} M and (d′) 1×10^{-2} M; potential = 6.0 mV. Similarly, (B) represents [LC] = (a′) 1×10^{-5} M; (b′) 1×10^{-4} M and (c′) 1×10^{-3} M; potential = 58.0 mV. In both of these experiments the carrier stream used was pH 8.4 TRIS aqueous buffer solution; flow rate = 0.03 ml s^{-1} and injected volume = 10 μl. The insets in (A) and (B) show the plot of current vs. different concentration of analytes, respectively at MWCNTs–DNA–cyt *c* biocomposite films.

is $-0.6\,\mu A\,mM^{-1}$ for IO_3^-, $-0.8\,\mu A\,mM^{-1}$ for BrO_3^- and $-0.01\,\mu A\,mM^{-1}$ for ClO_3^- with a correlation coefficient of 0.8879, 0.9998 and 0.8506, respectively, where $n = 4$. From these values, the sensitivity of the sensor has been calculated and it was -0.38, -0.51 and $-0.006\,\mu A\,mM^{-1}\,cm^{-2}$ for IO_3^-, BrO_3^- and ClO_3^-, respectively. Those insets also represent error bars, where each concentration of each analytes has been studied three times. These error bars showed that the MWCNTs–DNA–cyt *c* biocomposite films have good reproducibility for each analyte.

Similar MWCNTs–DNA–cyt *c* modified SPCEs have been prepared at similar conditions for the FIA of AA and LC. The experimental conditions have been similar to that of halogen oxyanions, however here, the pH 8.4 TRIS aqueous buffer solution was used as the carrier stream. Fig. 7(A) shows the successive addition of (A) AA and (B) LC in the concentration range from 0.1 to 10 mM at the potential of 6.0 mV for AA and 58.0 mV for LC, and these are the optimized potentials obtained from CV studies. The rapid amperometric response of the MWCNTs–DNA–cyt *c* biocomposite film is proportional to the respective analytes concentration. The insets show the slope obtained for AA is $0.03\,\mu A\,mM^{-1}$ and LC is $0.02\,\mu A\,mM^{-1}$ with a correlation coefficient of 0.9239 and 1.0, respectively, where $n = 4$ for AA and 3 for LC. From these values, the sensitivity of the sensor has been calculated and it was 0.02 and $0.01\,\mu A\,mM^{-1}\,cm^{-2}$ for AA and LC, respectively. These insets also represent error bars, similar to that of halogen oxyanions FIA, which showed that the MWCNTs–DNA–cyt *c* biocomposite films have good reproducibility for each analytes.

4. Conclusions

In conclusion, we have developed a novel biocomposite material with MWCNTs, DNA and cyt *c* (MWCNTs–DNA–cyt *c*) at the GCE, Au, ITO and SPCE electrode surfaces, which are more stable in aqueous solutions of pH 8.4 TRIS buffer and pH 1 H_2SO_4. The developed biocomposite film for the electrocatalysis, combines the advantages of ease of fabrication, high reproducibility and sufficient long-term stability. The EQCM results has confirmed the incorporation of cyt *c* on MWCNTs–DNA modified gold electrode, SEM and AFM results have shown the difference between cyt *c*, DNA–cyt *c*, MWCNTs–cyt *c* and MWCNTs–DNA–cyt *c* biocomposite films morphological data. The interactions between the MWCNTs, DNA and cyt *c* are presented with the scheme. Further, it has been found that the MWCNTs–DNA–cyt *c* biocomposite film has an excellent functional property along with good electrocatalytic activity on halogen oxyanions and biochemical compounds such as ascorbic acid and L-cysteine. The electrocatalytic reduction of halogen oxyanions such as IO_3^-, BrO_3^- and ClO_3^- and its electronegativity effect on electrocatalysis have also been studied in detail. The interactions between the analytes and the MWCNTs–DNA–cyt *c* biocomposite film have been given in equations with previous literature references. The experimental methods of CV and FIA with biocomposite film biosensor integrated into the GCE and SPCE which are presented in this paper, provide an opportunity for qualitative and quantitative characterization, even at physiologically relevant conditions. Therefore, this work establishes and illustrates, in principle and potential, a simple and novel approach for the development of a voltammetric and amperometric sensor which is based on the modified GCE, ITO, Au and SPCE electrodes.

Acknowledgement

This work was supported by the National Science Council of the Taiwan (ROC).

Appendix A. Supplementary data

Supplementary data associated with this article can be found, in the online version, at doi:10.1016/j.talanta.2007.10.034.

References

[1] E.F. Bowden, F.M. Hawkridge, H.N. Blount, J. Electroanal. Chem. 161 (1984) 355.
[2] H.A.O. Hill, N.I. Hunt, A.M. Bond, J. Electroanal. Chem. 436 (1997) 17.
[3] P. Yeh, T. Kuwana, Chem. Lett. (1977) 1145.
[4] M.J. Eddowes, H.A.O. Hill, J. Chem. Soc., Chem. Commun. 771 (1977) 364.
[5] A. Szucs, G.D. Hitchens, J.O.'M. Bockris, Electrochim. Acta 37 (1992) 403.
[6] G. Battistuzzi, M. Borsari, G. Rossi, M. Sola, Inorg. Chim. Acta 272 (1998) 168.
[7] A. Szues, M. Novak, J. Electroanal. Chem. 383 (1995) 75.
[8] Z.X. Huang, M. Feng, Y.H. Wang, J. Cui, D.S. Zou, J. Electroanal. Chem. 416 (1996) 31.
[9] M.J. Eddowes, H.A.O. Hill, J. Am. Chem. Soc. 101 (1979) 4461.
[10] F.A. Armstrong, H.A.O. Hill, N.J. Walton, Acc. Chem. Res. 21 (1988) 407.
[11] S. Dong, J. Li, Bioelectrochem. Bioenerg. 42 (1997) 7.
[12] Y. Zhou, T. Nagaoka, G. Zhu, Biophys. Chem. 79 (1999) 55.
[13] G. Niaura, A.K. Gaigalas, V.L. Viker, J. Electroanal. Chem. 416 (1996) 167.
[14] O. Ikeda, Y. Shirota, T. Sakurai, J. Electroanal. Chem. 287 (1990) 179.
[15] X. Qu, T. Lu, S. Dong, J. Mol. Catal. A: Chem. 102 (1995) 111.
[16] E.D.A. Stemp, J.K. Barton, Inorg. Chem. 39 (2000) 3868.
[17] A.E.F. Nassar, J.F. Rusling, J. Am. Chem. Soc. 118 (1996) 3043.
[18] S.M. Chen, S.V. Chen, Electrochim. Acta 48 (2003) 513.
[19] U. Yogeswaran, S.M. Chen, Electrochim. Acta 52 (2007) 5985.
[20] G. Wu, Y.S. Chen, B.Q. Xu, Electrochem. Commun. 7 (2005) 1237.
[21] J. Wang, M. Musameh, Anal. Chim. Acta 511 (2004) 33.
[22] J. Wang, M. Li, Z. Shi, N. Li, Z. Gu, Electrochim. Acta 47 (2001) 651.
[23] Q. Li, J. Zhang, H. Yan, M. He, Z. Liu, Carbon 42 (2004) 287.
[24] J. Zhang, J.K. Lee, Y. Wu, R.W. Murray, Nano Lett. 3 (2003) 403.
[25] A. Star, T.R. Han, J. Christophe, P. Gabriel, K. Bradley, G. Gruner, Nano Lett. 3 (2003) 1421.
[26] M. Zhang, K. Gong, H. Zhang, L. Mao, Biosens. Bioelectron. 20 (2005) 1270.
[27] R.J. Chen, Y. Zhang, D. Wang, H. Dai, J. Am. Chem. Soc. 123 (2001) 3838.
[28] Y. Yan, M. Zhang, K. Gong, L. Su, Z. Guo, L. Mao, Chem. Mater. 17 (2005) 3457.
[29] G. Han, J. Yuan, G. Shi, F. Wei, Thin Solid Films 474 (2005) 64.
[30] U. Yogeswaran, S. Thiagarajan, S.M. Chen, Anal. Biochem. 365 (2007) 122.
[31] E. Frackowiak, V. Khomenko, K. Jurewicz, K. Lota, F. Béguin, J. Power Sources 153 (2006) 413.
[32] S. Daniel, T.P. Rao, K.S. Rao, S.U. Rani, G.R.K. Naidu, H.Y. Lee, T. Kawai, Sens. Actuators B 122 (2007) 672.
[33] S.M. Chen, M.I. Liu, Electrochim. Acta 51 (2006) 4744.
[34] S.M. Chen, C.J. Liao, V.S. Vasantha, J. Electroanal. Chem. 589 (2006) 15.

[35] J. Wang, J. Dai, T. Yarlagadda, Langmuir 21 (2005) 9.
[36] M. Tahhan, V.T. Truong, G.M. Spinks, G.G. Wallace, Smart Mater. Struct. 12 (2003) 626.
[37] E. Laviron, J. Electroanal. Chem. 101 (1979) 19.
[38] T. Komura, G.Y. Niu, T. Yamaguchi, M. Asano, A. Matsuda, Electroanalysis 16 (2004) 1791.
[39] A. Mohadesi, M.A. Taher, Sens. Actuators B 123 (2007) 733.
[40] S.M. Chen, K.C. Lin, J. Electroanal. Chem. 511 (2001) 101.
[41] C.P. Andrieux, O. Haas, J.M. SavGant, J. Am. Chem. Soc. 108 (1986) 8175.
[42] S. Imabayashi, T. Mita, T. Kakiuchi, Langmuir 21 (2005) 1470.
[43] X. Ji, J. Ren, J. Jin, T. Nakamur, Biosens. Bioelectron. 23 (2007) 241.
[44] F. d'Souza, L.M. Rogers, E.S. O'Dell, A. Kochman, W. Kutner, Bioelectrochemistry 66 (2005) 35.
[45] S.F. Ding, W. Wei, G.C. Zhao, Electrochem. Commun. 9 (2007) 2202.
[46] L. Zhang, X. Jiang, L. Niu, S. Dong, Biosens. Bioelectron. 21 (2006) 1107.
[47] A.F. Runge, S.S. Saavedra, Langmuir 19 (2003) 9418.
[48] D.H. Murgida, P. Hildebrandt, J. Phys. Chem. B 105 (2001) 1578.